

# Identification-based Closed-loop NMES Limb Tracking with **Amplitude**-Modulated Control Input

T. -H. Cheng<sup>1</sup>, Q. Wang<sup>2</sup>, R. Kamalapurkar<sup>1</sup>, H. T. Dinh<sup>1</sup>, M. Bellman<sup>1</sup>, and W. E. Dixon<sup>1,2</sup>

**Abstract**—An upper motor neuron lesion (UMNL) can be caused by various neurological disorders or trauma and leads to disabilities. Neuromuscular electrical stimulation (NMES) is a technique that is widely used for rehabilitation and restoration of motor function for people suffering from UMNL. Typically, stability analysis for closed-loop NMES ignores the modulated implementation of NMES. However, electrical stimulation must be applied to muscle as a modulated series of pulses. In this paper, a muscle activation model with an **amplitude** modulated control input is developed to capture the discontinuous nature of muscle activation, and an identification-based closed-loop NMES controller is designed and analyzed for the uncertain **amplitude modulated** muscle activation model. Semi-global uniformly ultimately bounded (SUUB) tracking is guaranteed. The stability of the closed-loop system is analyzed with Lyapunov-based methods, and a pulse frequency related gain condition is obtained. Experiments are performed with five able-bodied subjects to demonstrate the interplay between the control gains and the pulse frequency, and results are provided which indicate that control gains should be increased to maintain stability if the stimulation pulse frequency is decreased to mitigate muscle fatigue. For the first time, this paper brings together an analysis of the controller and modulation scheme.

## I. INTRODUCTION

Upper motor neuron lesions (UMNL) cause disability and paralysis in millions of people. UMNL is usually caused by neural disorders such as stroke or cerebrovascular accident, spinal cord injury, multiple sclerosis, cerebral palsy, or traumatic brain injury. The overall reported prevalence is 37,000 people/million/year for an UMNL [1]. Since the lower motor neuron system and muscles are intact in those with UMNL, muscle contractions can be evoked by directly applying electrical stimulus to the muscles; this technique is widely used for rehabilitation and restoration of motor function and is referred to as neuromuscular electrical stimulation (NMES) or functional electrical stimulation (FES) when applied to produce a functional outcome. The development of an NMES method to provide a desired outcome is challenging due to the nonlinear response from muscle to electrical input, load changes during functional movement, unexpected muscle spasticity, time lag between muscle activation and muscle

force output, and muscle fatigue. Closed-loop NMES control is promising with regard to its ability to achieve precise limb movement and disturbance rejection, both of which are essential for functional rehabilitation.

Several PID (proportional–integral–derivative) based linear NMES controllers have been developed [2]–[5], but these methods typically rely on a linear muscle model and lack a stability analysis. Neural network (NN) based NMES controllers [6]–[19] have been developed which utilize the universal approximation property of NNs to approximate the nonlinear (unstructured) dynamics. Robust NMES methods have been developed in [20] and [21] that achieve guaranteed asymptotic limb tracking. In [22] and [23], inverse and direct optimal NMES controllers were developed with guaranteed stability, and the authors addressed the problem of muscle fatigue from overstimulation by balancing the performance and the control effort. In [5] and [24], muscle contraction dynamics were modeled with known parameters or with best estimates of the parameters, and nonlinear controllers were developed which yielded asymptotically stable closed-loop error systems. In [25], the control method used model-free, adaptive pattern generator/pattern shapers (PG/PS), but stability analysis of the closed-loop error system was not analyzed. In [17], an adaptive, neuro-sliding-mode controller was developed based on uncertain human knee-joint dynamics, and it was demonstrated in able-bodied and paralyzed individuals that the developed controller was able to successfully track a desired knee-joint trajectory. In [26], an adaptive robust control system for FES-induced ankle dorsiflexion and plantarflexion was developed based on fuzzy logic and sliding mode control methods that yielded accurate tracking performance of an ankle trajectory in able-bodied and paraplegic subjects without requiring a priori model knowledge. In [27], the control system developed in [26] was extended to the task of walker-assisted FES-walking with FES controllers for the hip, knee, and ankle joints. Despite the success of these previous approaches, controllers were developed without accounting for how the control signal is modulated during application to the muscle. **Previous approaches assumed that the stimulation applied across the muscle groups is continuous. However, in practice, stimulation is typically applied in the form of discrete pulses, and the pulse amplitude, duration, and frequency is modulated to control the muscle force output during FES. Since modulation strategies are not considered in any previous system models, the developed controllers and subsequent stability analyses, if performed, yield no insight into the interplay**

1. Department of Mechanical and Aerospace Engineering, University of Florida, Gainesville FL 32611-6250, USA Email: {tenghu, rkamalapurkar, huyentdihn, mattjo wdixon}@ufl.edu

2. Department of Electrical and Computer Engineering, University of Florida, Gainesville FL 32611-6250, USA Email: {qiangw, wdixon}@ufl.edu

This research is supported in part by NSF award numbers 1161260 and 1217908. Any opinions, findings and conclusions or recommendations expressed in this material are those of the author(s) and do not necessarily reflect the views of the sponsoring agency.

between the controller and the modulation parameters.

NMES is delivered in the form of electrical pulses which create a localized electric field to elicit action potentials in the nearby neurons. Muscle force output is determined by the pulse amplitude, duration, frequency, and the muscle fatigue state. Pulse duration and amplitude determine the activation region, i.e., how many motor units are recruited, and are equivalent with regard to the total applied electric charge. This effect is often referred to as spatial summation. Each electric pulse causes a twitch in the muscle fibers. If a second pulse is applied before the first twitch finishes, the two twitches sum and a higher force output from the muscle is achieved. This effect is often referred to as temporal summation. When the pulse frequency is higher than a threshold called the fusion frequency, continuous muscle force output is observed, and larger forces can be achieved with higher frequencies. However, higher stimulation frequencies cause the muscle to fatigue faster. In practice, muscle force is controlled by modulating the pulse amplitude or pulse duration, and the frequency is set to a constant value that is as low as possible to maintain fused force output while avoiding fatiguing the muscle prematurely [28]. Recent results demonstrated that frequency-modulation can yield better performance for both peak forces and force-time integrals than pulse-duration-modulation, while producing similar levels of muscle fatigue [29]. **However, it is still unclear how different amplitude-modulation strategies affect the performance of FES-induced activities and what modulation strategy should be used to maximize performance.**

In [30], an identification-based controller was developed for the muscle-limb model which includes an uncertain first-order dynamic system that models muscle contraction dynamics. The parameters of the limb dynamics and the muscle contraction model are unknown. Since the NMES control input is implemented as a series of pulses and the modulation strategy has significant impact on the muscle performance and fatigue, the ability to examine the impact of the control signal and modulation strategy analytically may yield new insights into the development of NMES controllers. In this paper, a muscle activation model with a **amplitude**-modulated control input is developed to capture the discontinuous nature of muscle activation, and an identification-based closed-loop NMES controller is designed and analyzed for the uncertain pulse muscle activation model. Semi-global uniformly ultimately bounded (SUUB) tracking is guaranteed through Lyapunov-based methods. A sufficient condition for stability that relates the pulse frequency and the control gains is obtained. Experiments are performed with five able-bodied subjects to demonstrate the interplay between the control gains and the pulse frequency, and results are provided which indicate that control gains should be increased to maintain tracking performance if the stimulation pulse frequency is decreased to mitigate muscle fatigue.

## II. DESCRIPTION OF THE DYNAMICS

A freely swinging lower limb with respect to the knee-joint can be segregated into body segmental dynamics and muscle activation and contraction dynamics. The body segmental dynamics can be expressed as

$$M_I(\ddot{q}) + M_e(q) + M_g(q) + M_v(\dot{q}) + \tau_d = \tau_m, \quad (1)$$

where  $q, \dot{q}, \ddot{q} \in \mathbb{R}$  denote the angular position, velocity, and acceleration of the lower limb about the knee-joint, respectively;  $\tau_m : [0, \infty) \rightarrow \mathbb{R}$  denotes the active torque at the knee-joint produced by muscle through electrical stimulation;  $M_I : \mathbb{R} \rightarrow \mathbb{R}$  denotes the inertial effects of the lower limb-foot complex about the knee-joint;  $M_e : \mathbb{R} \rightarrow \mathbb{R}$  denotes the elastic effects due to joint stiffness;  $M_g : \mathbb{R} \rightarrow \mathbb{R}$  denotes the gravitational component;  $M_v : \mathbb{R} \rightarrow \mathbb{R}$  denotes the viscous effects due to damping in the musculotendon complex [31]; and  $\tau_d : [0, \infty) \rightarrow \mathbb{R}$  includes all other unmodeled effects and disturbances such as external loads. In (1) and in the subsequent development, the dependence on time is suppressed, The inertial component  $M_I$  in (1) is defined as

$$M_I(\ddot{q}) \triangleq J_I \ddot{q}, \quad (2)$$

where  $J_I \in \mathbb{R}$  is an unknown constant, denoted as the inertia of the lower limb-foot complex about the knee-joint. The total muscle torque  $\tau_m$  generated at the knee-joint is considered as an unknown nonlinear function  $\zeta : \mathbb{R} \rightarrow \mathbb{R}$  (which is the moment arm) multiplied by the muscle contraction force  $x_f : \mathbb{R} \times \mathbb{R} \rightarrow \mathbb{R}$  generated by electric stimulation as

$$\tau_m \triangleq \zeta(q) x_f(q, \dot{q}). \quad (3)$$

The elastic effects are modeled on the empirical findings by Ferrarin and Pedotti in [31] as

$$M_e(q) = -K_1(e^{-K_2 q})(q - K_3),$$

where  $K_1, K_2, K_3 \in \mathbb{R}$  are unknown positive constants. As in [5], the viscous moment  $M_v$  can be modeled as

$$M_v(\dot{q}) = B_1 \tanh(-B_2 \dot{q}) - B_3 \dot{q},$$

where  $B_1, B_2, B_3 \in \mathbb{R}$  are unknown positive constants. For complete details of the dynamics in (1), see [21].

The following assumptions and properties are used to facilitate the subsequent control development and stability analysis.

**Property 1.** The moment arm  $\zeta$  is a continuously differentiable, nonzero, positive, monotonic, and bounded function [32].

**Assumption 1.** The disturbance term  $\tau_d$  and its time derivatives  $\dot{\tau}_d, \ddot{\tau}_d$  are bounded.

The model developed in (1)–(3) is used to examine the stability of the subsequently developed controller, but the controller does not explicitly depend on the model. After

substituting (2) and (3), and dividing both sides by  $\zeta$ , the expression in (1) can be written as

$$\zeta^{-1}(q) J_I \ddot{q} + \zeta^{-1}(q) (M_e(q) + M_g(q) + M_v(\dot{q})) + \zeta^{-1}(q) \tau_d = x_f(q, \dot{q}). \quad (4)$$

Muscle activation and contraction dynamics can be modeled as in [5], [24], [33], [34], which can be generalized as

$$\dot{x}_f(q, \dot{q}, \ddot{q}) + A_f(q, \dot{q}) x_f(q, \dot{q}) + f_1(q, \dot{q}, \ddot{q}) + \tau_1 = b(q, \dot{q}) u, \quad (5)$$

where  $A_f, f_1 : \mathbb{R} \times \mathbb{R} \rightarrow \mathbb{R}$  and  $b : \mathbb{R} \times \mathbb{R} \times \mathbb{R} \rightarrow \mathbb{R}$  are uncertain continuous functions,  $\tau_1 : [0, \infty) \rightarrow \mathbb{R}$  represents disturbances in the muscle (e.g., muscle spasticity, fatigue, and volitional muscle activation), and  $u : [0, \infty) \rightarrow \mathbb{R}$  is the applied electric stimulation voltage. The first-order, nonlinear differential equation in (5) represents a generalization of the relationship between the excitation input,  $u$ , and muscle fiber force output,  $x_f$ , which combines the muscle activation and contraction dynamics based on the models in [24], [25], [33]. The introduction of the unknown nonlinear functions  $A_f, f_1$  enables the muscle contraction to be considered under general conditions in the subsequent control development.

**Property 2.** Based on the empirical data in [35] and [36], the muscle gain (recruiting) function  $b$  is a bounded, positive function with bounded, first-order time derivatives.

By substituting  $x_f$  and  $\dot{x}_f$  into (5), the dynamics in (5) can be expressed as

$$J(q, \dot{q}, \ddot{q}) \ddot{q} = -f_2(q, \dot{q}, \ddot{q}) - \tau_2 + u, \quad (6)$$

where  $J, f_2 : \mathbb{R} \times \mathbb{R} \times \mathbb{R} \rightarrow \mathbb{R}$  and  $\tau_2 : [0, \infty) \rightarrow \mathbb{R}$  are defined as

$$\begin{aligned} J(q, \dot{q}, \ddot{q}) &\triangleq b^{-1}(q, \dot{q}) \zeta^{-1}(q) J_I, \\ f_2(q, \dot{q}, \ddot{q}) &\triangleq b^{-1}(q, \dot{q}) \left( -J_I \zeta^{-2}(q) \dot{\zeta}(q, \dot{q}) \right. \\ &\quad + A_f(q, \dot{q}) J_I \zeta^{-1}(q) \ddot{q} + b^{-1}(q, \dot{q}) \\ &\quad \times f_1(q, \dot{q}, \ddot{q}) + b^{-1}(q, \dot{q}) \zeta^{-1}(q) A_f(q, \dot{q}) \\ &\quad \times (M_e(q) + M_g(q) + M_v(\dot{q})) \\ &\quad + b^{-1}(q, \dot{q}) \zeta^{-1}(q) \left( \dot{M}_e(q, \dot{q}) \right. \\ &\quad \left. + \dot{M}_g(q, \dot{q}) + \dot{M}_v(\dot{q}, \ddot{q}) \right) \\ &\quad \left. - b^{-1}(q, \dot{q}) \zeta^{-2}(q) \dot{\zeta}(q, \dot{q}) \right. \\ &\quad \left. \times (M_e(q) + M_g(q) + M_v(\dot{q})) \right), \quad (7) \\ \tau_2 &\triangleq b^{-1}(q, \dot{q}) \left( \dot{\tau}_d \zeta^{-1}(q) - \tau_d \zeta^{-2}(q) \dot{\zeta}(q, \dot{q}) \right. \\ &\quad \left. + \tau_1 + A_f(q, \dot{q}) \tau_d \zeta^{-1}(q) \right). \end{aligned}$$

Based on Properties 1-2, the following inequalities can be developed

$$\xi_0 \leq J(q, \dot{q}, \ddot{q}) \leq \xi_1, \quad |\tau_2| \leq \xi_2, \quad (8)$$

where  $\xi_i \in \mathbb{R}$ ,  $i = 0, 1, 2$  are known positive constants.

The electrical pulse input  $u$  can be modeled as

$$u = \begin{cases} v, & nT \leq t < nT + d \\ v_b, & \text{otherwise} \end{cases}, \quad (9)$$

$$n = 0, 1, 2, \dots$$

where  $v : [0, \infty) \rightarrow \mathbb{R}$  and  $d, T \in \mathbb{R}$  denote pulse amplitude, width, and period<sup>1</sup>, respectively, and  $v_b : [0, \infty) \rightarrow \mathbb{R}$  is a stimulation signal for the balanced charged purpose and  $v_b$  is bounded by  $|v_b| \leq \bar{v}_b \in \mathbb{R}_{\geq 0}$ . In other words, the controller is modulated in the sense that  $u = v$  when  $t$  satisfies  $nT \leq t < nT + d$ , whereas  $u = 0$  at  $nT + d < t < (n+1)T$ . The pulse frequency is defined as  $f \triangleq \frac{1}{T}$ . Based on (9) the system in (6) can be expressed as

$$J \ddot{q} = \begin{cases} -f_2(q, \dot{q}, \ddot{q}) - \tau_2 + v, & nT \leq t < nT + d \\ -f_2(q, \dot{q}, \ddot{q}) - \tau_2 + v_b, & \text{otherwise} \end{cases}, \quad (10)$$

$$n = 0, 1, 2, 3, \dots$$

### III. CONTROLLER DEVELOPMENT

The control objective is to ensure the knee angle  $q$  tracks a desired trajectory, denoted by  $q_d : [0, \infty) \rightarrow \mathbb{R}$ , which is an essential task in many rehabilitative exercises and function restoration tasks. To quantify the tracking objective, a lower limb angular position tracking error, denoted by  $e : [0, \infty) \rightarrow \mathbb{R}$ , is defined as

$$e \triangleq q_d - q, \quad (11)$$

where  $q_d$  is a known trajectory, designed such that  $q_d, q_d^i \in \mathcal{L}_\infty$ , where  $q_d^i$  denotes the  $i^{\text{th}}$  derivative of  $q_d$  for  $i = 1, 2, 3$ . To facilitate the subsequent control design and stability analysis, filtered tracking errors denoted by  $e_1, e_2 : [0, \infty) \rightarrow \mathbb{R}$ , are also defined as

$$e_1 \triangleq \dot{e} + \alpha_1 e, \quad (12)$$

$$e_2 \triangleq \dot{e}_1 + \alpha_2 e_1, \quad (13)$$

where  $\alpha_1, \alpha_2 \in \mathbb{R}$  are positive constant control gains. Using (11)–(13),  $e_2$  can be expressed as

$$e_2 = \ddot{q}_d - \ddot{q} + (\alpha_1 + \alpha_2) (\dot{q}_d - \dot{q}) + \alpha_1 \alpha_2 e. \quad (14)$$

The subsequent development is based on the assumption that  $q$  and  $\dot{q}$  are measurable. The error dynamics in (14) depend on the unmeasurable limb acceleration. To compensate for the acceleration dependency, an acceleration estimation error  $\hat{e}_2 : [0, \infty) \rightarrow \mathbb{R}$  is designed based on (14) as

$$\hat{e}_2 \triangleq \ddot{q}_d - \ddot{q} + (\alpha_1 + \alpha_2) (\dot{q}_d - \dot{q}) + \alpha_1 \alpha_2 e, \quad (15)$$

where  $\hat{q}, \hat{\dot{q}} : [0, \infty) \rightarrow \mathbb{R}$  denote the subsequently designed observer outputs.

<sup>1</sup>In this paper, monophasic stimulation pulses were considered for simplicity, but the proposed method could be extended to variable frequency and n-let pulse trains, including biphasic, charge-balanced pulse trains, which are typically used in FES applications.

To facilitate the subsequent analysis, let  $f_{2d} : \mathbb{R} \times \mathbb{R} \times \mathbb{R} \rightarrow \mathbb{R}$  be defined as

$$f_{2d}(q_d, \dot{q}_d, \ddot{q}_d) \triangleq f_2(q_d, \dot{q}_d, \ddot{q}_d) \quad (16)$$

where  $f_{2d}$  is the same function as  $f_2$ , except that its arguments  $q$ ,  $\dot{q}$ , and  $\ddot{q}$  are replaced by the desired arguments  $q_d$ ,  $\dot{q}_d$ , and  $\ddot{q}_d$ . Using the bounded desired arguments ensures that the domain of  $f_{2d}$  is a compact set, which is a requirement for neural network approximation. Based on the universal function approximation property [37], the unknown function in (16) can be approximated by a multi-layer NN as

$$f_{2d}(q_d, \dot{q}_d, \ddot{q}_d) = W^T \sigma(V^T X_d) + \varepsilon(q_d, \dot{q}_d, \ddot{q}_d), \quad (17)$$

where  $X_d \in \mathbb{R}^4$  is defined as

$$X_d \triangleq [1, q_d, \dot{q}_d, \ddot{q}_d]^T;$$

$\sigma : \mathbb{R}^{n_0} \rightarrow \mathbb{R}^{n_0+1}$  denotes the activation function;  $W \in \mathbb{R}^{n_0+1}$ ,  $V \in \mathbb{R}^{4 \times n_0}$  denote the bounded constant ideal weights for the hidden layer neurons and the input layer neurons, respectively, where the number of hidden layer neurons is selected as  $n_0$ ; and  $\varepsilon : \mathbb{R} \times \mathbb{R} \times \mathbb{R} \rightarrow \mathbb{R}$  denotes the reconstruction error.

**Assumption 2.** The activation function  $\sigma$  and its first order derivative with respect to its arguments  $\sigma'$  are bounded by known constants [38].

**Property 3.** The reconstruction error  $\varepsilon$  and its first order partial derivative  $\varepsilon'$  are bounded by known constants [38].

For notational brevity the dependence of all the functions on the states is suppressed hereafter.

After multiplying the time derivative of (14) by  $J$ , and using (6), (11)-(13), (16), and (17), the open-loop error system for  $e_2$  is

$$\begin{aligned} J\dot{e}_2 &= -\frac{1}{2}J\dot{e}_2 + f_2 - f_{2d} + W^T \sigma(V^T X_d) \\ &+ \frac{1}{2}J\dot{e}_2 - J\alpha_1^2 \dot{e} + J(\alpha_1 + \alpha_2) \dot{e}_1 \\ &+ J\ddot{q}_d + \tau_2 + \varepsilon - u. \end{aligned} \quad (18)$$

Let  $\hat{W} : [0, \infty) \rightarrow \mathbb{R}^{n_0+1}$ ,  $\hat{V} : [0, \infty) \rightarrow \mathbb{R}^{4 \times n_0}$  denote the estimated weights for  $W$ ,  $V$ , and let  $\sigma$ ,  $\hat{\sigma}$ ,  $\hat{\sigma}'$ ,  $\tilde{\sigma}$ ,  $\tilde{W} \in \mathbb{R}^{n_0}$ ,  $\tilde{V} \in \mathbb{R}^{4 \times n_0}$  be defined as

$$\sigma \triangleq \sigma(V^T X_d), \quad (19)$$

$$\hat{\sigma} \triangleq \sigma(\hat{V}^T X_d), \quad (20)$$

$$\hat{\sigma}' \triangleq \frac{\partial(\sigma(\hat{V}^T X))}{\partial(\hat{V}^T X)} \Big|_{\hat{V}^T X = \hat{V}^T X_d}, \quad (21)$$

$$\tilde{\sigma} \triangleq \sigma - \hat{\sigma}, \quad (22)$$

$$\tilde{W} \triangleq W - \hat{W}, \quad (23)$$

$$\tilde{V} \triangleq V - \hat{V}. \quad (24)$$

By using a Taylor series approximation,  $\tilde{\sigma}$  can be expressed as  $\tilde{\sigma} = \hat{\sigma}' \tilde{V}^T X_d + o(\tilde{V}^T X_d)^2$ , where  $o(\cdot)^2 \in \mathbb{R}^{n_0}$  denotes

higher order terms. By using (19)–(24),  $W^T \sigma$  can be expressed as

$$\begin{aligned} W^T \sigma &= \hat{W}^T \hat{\sigma}' \tilde{V}^T X_d + W^T \hat{\sigma} \\ &+ \tilde{W}^T \hat{\sigma}' \tilde{V}^T X_d + W^T o(\tilde{V}^T X_d)^2. \end{aligned} \quad (25)$$

The update laws  $\dot{\hat{W}} \in \mathbb{R}^{n_0+1}$ ,  $\dot{\hat{V}} \in \mathbb{R}^{4 \times n_0}$  can be arbitrarily selected as

$$\dot{\hat{W}} \triangleq \text{proj}(\cdot), \quad \dot{\hat{V}} \triangleq \text{proj}(\cdot), \quad (26)$$

where  $\text{proj}(\cdot)$  is a smooth projection operator (e.g., see Section 4.3 of [39]). Gradient-based update laws were used in the following experiments. Since  $\text{proj}(\cdot)$  guarantees  $\hat{W}$ ,  $\hat{V}$  are bounded,

$$\left| \hat{W}^T \hat{\sigma} \right| \leq a_1, \quad (27)$$

where  $a_1 \in \mathbb{R}$  is a known positive constant.

The error system in (18) can be expressed as

$$J\dot{e}_2 = -\frac{1}{2}J\dot{e}_2 + f_3 + \hat{W}^T \hat{\sigma} - u, \quad (28)$$

where the auxiliary function  $f_3 \in \mathbb{R}$  is defined as

$$\begin{aligned} f_3 &\triangleq f_2 - f_{2d} + \tilde{W}^T \hat{\sigma} \\ &+ \hat{W}^T \hat{\sigma}' \tilde{V}^T X_d + \tilde{W}^T \hat{\sigma}' \tilde{V}^T X_d \\ &+ W^T o(\tilde{V}^T X_d)^2 \\ &- J\alpha_1^2 \dot{e} + J(\alpha_1 + \alpha_2) \dot{e}_1 \\ &+ \frac{1}{2}J\dot{e}_2 + J\ddot{q}_d + \varepsilon + \tau_2. \end{aligned}$$

Since  $W$ ,  $V$ ,  $\sigma$ , and  $\varepsilon$  are bounded, using the Mean Value Theorem, (26), and the assumption that  $\ddot{q}_d$  is bounded,  $f_3$  can be bounded as

$$|f_3| \leq a_2 + \rho_1 (\|z_f\|) \|z_f\|, \quad (29)$$

where  $a_2 \in \mathbb{R}$  is a positive constant,  $z_f \in \mathbb{R}^3$  is defined as  $z_f \triangleq (e, e_1, e_2)^T$ , and  $\rho_1 : [0, \infty) \rightarrow [0, \infty)$  is a positive, strictly increasing, and radially unbounded function<sup>2</sup>. Based on (26), (28), and the subsequent stability analysis, the control input is designed as

$$v = k_f \hat{e}_2 + \hat{W}^T \hat{\sigma}, \quad (30)$$

where  $k_f \in \mathbb{R}$  is a positive control gain.

After substituting (9) and (30) into (28), the closed-loop error system can be obtained as

$$J\dot{e}_2 = \begin{cases} -\frac{1}{2}J\dot{e}_2 + f_3 - k_f \hat{e}_2, & nT \leq t < nT + d \\ -\frac{1}{2}J\dot{e}_2 + f_3 + \hat{W}^T \hat{\sigma} + v_b, & \text{otherwise} \end{cases}, \quad (31)$$

$n = 0, 1, 2, 3, \dots$

<sup>2</sup>For some classes of systems, the bounding function  $\rho_1$  could be selected as a constant, and a global uniformly ultimately bounded result can be obtained.

#### IV. OBSERVER DESIGN

The objective of this section is to design an observer/identifier to generate estimations of  $\hat{q}$  and  $\dot{q}$ , which are used to generate  $\hat{e}_2$  in (15), so that the controller in (30) can be implemented with only measurements of  $q$  and  $\dot{q}$ .

To facilitate the observer design, let  $x, \hat{x}, \tilde{x}, r \in \mathbb{R}^2$ ,  $z \in \mathbb{R}^4$  be defined as

$$x \triangleq [q, \dot{q}]^T, \quad (32)$$

$$\hat{x} \triangleq \begin{bmatrix} \hat{q} \\ \dot{\hat{q}} \end{bmatrix}^T, \quad (33)$$

$$\tilde{x} \triangleq x - \hat{x}, \quad (34)$$

$$r \triangleq [r_1, r_2]^T \quad (35)$$

$$= \dot{\hat{x}} + \alpha \tilde{x}, \quad (36)$$

$$z \triangleq [\tilde{x}^T, r^T]^T, \quad (37)$$

where  $\alpha \triangleq \alpha_1 + \alpha_2$ . By using (13) and (15), the difference between  $e_2$  and  $\hat{e}_2$  is

$$r_2 = \hat{e}_2 - e_2. \quad (38)$$

After substituting (2) and (3), the dynamics in (1) can be expressed as

$$J_I \ddot{q} + M_e + M_g + M_v + \tau_d = \zeta x_f, \quad (39)$$

which can be rewritten as

$$\dot{x} = -\alpha x + g_1(q, \dot{q}) + h, \quad (40)$$

where  $x$  is defined in (32), and  $g_1 : \mathbb{R} \times \mathbb{R} \rightarrow \mathbb{R}^2$  and  $h : [0, \infty) \rightarrow \mathbb{R}^2$  are defined as

$$g_1(q, \dot{q}) \triangleq \alpha x + \begin{pmatrix} \dot{q} \\ -J_I^{-1}(M_e + M_g + M_v - \zeta x_f) \end{pmatrix},$$

$$h \triangleq \begin{pmatrix} 0 \\ -J_I^{-1}\tau_d \end{pmatrix}.$$

Let  $g_{1d} : \mathbb{R} \times \mathbb{R} \rightarrow \mathbb{R}^2$  be defined as  $g_{1d}(q_d, \dot{q}_d) \triangleq g_1(q_d, \dot{q}_d)$ . The unknown function  $g_{1d}$  can be approximated by a multi-layer NN with a reconstruction error as  $g_{1d}(q_d, \dot{q}_d) = W_1^T \sigma_1(V_1^T x_d) + \varepsilon_1(q_d, \dot{q}_d)$ , where  $x_d \in \mathbb{R}^2$  is defined as  $x_d \triangleq [q_d, \dot{q}_d]^T$ , and  $W_1 \in \mathbb{R}^{(n_1+1) \times 2}$ ,  $V_1 \in \mathbb{R}^{2 \times n_1}$  denote the ideal constant weights for the hidden layer neurons and the input layer neurons, respectively, where the number of hidden layer neurons is selected as  $n_1$ , and  $\varepsilon_1 : \mathbb{R} \times \mathbb{R} \rightarrow \mathbb{R}$  denotes the reconstruction error.

**Assumption 3.** The activation function  $\sigma_1 : \mathbb{R}^{n_1+1} \rightarrow \mathbb{R}^{n_1+1}$  and its first order derivative with respect to its arguments  $\sigma_1'$  are bounded by known constants [38].

**Property 4.** The reconstruction error  $\varepsilon_1$  and its first order derivative  $\varepsilon_1'$  are bounded by known constants [38].

The dynamics in (40) can be rewritten as

$$\dot{x} = -\alpha x + g_1 - g_{1d} + W_1^T \sigma_{1d} + \varepsilon_1 + h, \quad (41)$$

where  $\sigma_{1d} \triangleq \sigma_1(V_1^T x_d)$ . Based on (41), a multi-layer dynamic NN observer is designed as

$$\dot{\hat{x}} = -\alpha \hat{x} + \hat{W}_1^T \hat{\sigma}_1 + \mu, \quad (42)$$

where  $\hat{\sigma}_1 \triangleq \sigma_1(\hat{V}_1^T \hat{x})$ , and  $\hat{W}_1 : [0, \infty) \rightarrow \mathbb{R}^{(n_1+1) \times 2}$ ,  $\hat{V}_1 : [0, \infty) \rightarrow \mathbb{R}^{2 \times n_1}$  denote the estimated weights for  $W_1$ ,  $V_1$ , and  $\mu \in \mathbb{R}^2$  is defined as

$$\mu(\tilde{x}) \triangleq k\tilde{x} - k\tilde{x}(0) + \int_0^t k\alpha\tilde{x}d\tau, \quad (43)$$

where  $k \in \mathbb{R}$  is a positive control gain.

Based on (41) and (42), the observer error dynamics can be written as

$$\dot{\tilde{x}} = -\alpha\tilde{x} + \varepsilon_1 + \varepsilon_2 + g_1 - g_{1d} + h - \mu, \quad (44)$$

where  $\varepsilon_2 \in \mathbb{R}^2$  is defined as

$$\varepsilon_2 \triangleq W_1^T \sigma_{1d} - \hat{W}_1^T \hat{\sigma}_1. \quad (45)$$

After some algebraic manipulation, the time derivative of (45) can be written as

$$\begin{aligned} \dot{\varepsilon}_2 &= W_1^T \sigma_{1d}' V_1^T \dot{x}_d - \dot{W}_1^T \hat{\sigma}_1 \\ &\quad - \hat{W}_1^T \hat{\sigma}_1' \dot{\hat{V}}_1^T \hat{x} - W_1^T \hat{\sigma}_1' V_1^T \dot{\hat{x}} \\ &\quad + \tilde{W}_1^T \hat{\sigma}_1' \tilde{V}_1^T \dot{\hat{x}} + \hat{W}_1^T \hat{\sigma}_1' \tilde{V}_1^T \dot{\hat{x}} \\ &\quad + \tilde{W}_1^T \hat{\sigma}_1' \hat{V}_1^T \dot{\hat{x}}, \end{aligned} \quad (46)$$

where  $\tilde{W}_1 \triangleq W_1 - \hat{W}_1$ ,  $\tilde{V}_1 \triangleq V_1 - \hat{V}_1$  denote the mismatches for the ideal weight estimates,  $\sigma_{1d}' \triangleq \frac{\partial(\sigma_1(V_1^T x_d))}{\partial(V_1^T x_d)}$ , and  $\hat{\sigma}_1' \triangleq \frac{\partial(\sigma_1(\hat{V}_1^T \hat{x}))}{\partial(\hat{V}_1^T \hat{x})}$ . The update laws  $\dot{W}_1 \in \mathbb{R}^{(n_1+1) \times 2}$ ,  $\dot{V}_1 \in \mathbb{R}^{2 \times n_1}$  are designed as

$$\dot{W}_1 \triangleq \text{proj}(\Gamma_{w1} \hat{\sigma}_1' \hat{V}_1^T \dot{\hat{x}} \hat{x}^T), \quad (47)$$

$$\dot{V}_1 \triangleq \text{proj}(\Gamma_{v1} \dot{\hat{x}} \hat{x}^T \hat{W}_1^T \hat{\sigma}_1'), \quad (48)$$

where  $\Gamma_{w1} \in \mathbb{R}^{(n_1+1) \times (n_1+1)}$ ,  $\Gamma_{v1} \in \mathbb{R}^{2 \times 2}$  are positive definite gain matrices. The update laws in (47) and (48) ensure that

$$\alpha \tilde{x}^T \left( \hat{W}_1^T \hat{\sigma}_1' \tilde{V}_1^T \dot{\hat{x}} + \tilde{W}_1^T \hat{\sigma}_1' \hat{V}_1^T \dot{\hat{x}} \right) + \dot{G} = 0, \quad (49)$$

where  $G : [0, \infty) \rightarrow \mathbb{R}$  is defined as

$$G \triangleq \frac{\alpha}{2} \text{tr} \left( \tilde{W}_1^T \Gamma_{w1}^{-1} \tilde{W}_1 \right) + \frac{\alpha}{2} \text{tr} \left( \tilde{V}_1^T \Gamma_{v1}^{-1} \tilde{V}_1 \right).$$

By using the Mean Value Theorem, Assumptions 3-4, (47), and (48), the following inequalities can be obtained

$$N_1 \leq \rho_2 (\|\varphi\|) \|\varphi\| + a_3, \quad (50)$$

$$N_2 \leq a_4 \|z\| + a_5 \|z_f\| + a_6, \quad (51)$$

where  $N_1, N_2 \in \mathbb{R}$  are defined as

$$\begin{aligned} N_1(\varphi) &\triangleq W_1^T \sigma_1' V_1^T \dot{x}_d - \dot{W}_1^T \sigma_1 (\hat{V}_1^T \hat{x}) + \dot{\varepsilon}_1 + \dot{h} \\ &\quad - \dot{W}_1^T \hat{\sigma}_1' \hat{V}_1^T \hat{x} - W_1^T \hat{\sigma}_1' V_1^T \hat{x} + \tilde{W}_1^T \hat{\sigma}_1' \tilde{V}_1^T \hat{x} \\ &\quad + \dot{g}_1(q, \dot{q}, \ddot{q}) - \dot{g}_1(q_d, \dot{q}_d, \ddot{q}_d), \end{aligned} \quad (52)$$

$$N_2(\varphi) \triangleq \hat{W}_1^T \hat{\sigma}_1' \tilde{V}_1^T \hat{x} + \tilde{W}_1^T \hat{\sigma}_1' \hat{V}_1^T \hat{x}; \quad (53)$$

$a_3, a_4, a_5, a_6 \in \mathbb{R}$  are positive constants;  $\rho_2 : [0, \infty) \rightarrow [0, \infty)$  is a positive, strictly increasing, and radially unbounded function<sup>3</sup>; and  $\varphi \in \mathbb{R}^7$  is defined as  $\varphi \triangleq [z^T, z_f^T]^T$ . By using (32), (35), (46), (52), and (53), the observer error system in (44) can be rewritten as

$$\dot{r} = -kr + N_1 + N_2. \quad (54)$$

## V. STABILITY ANALYSIS

The stability of the overall system, depicted in Fig. 1, is subsequently analyzed based on Lyapunov methods for switched systems.

**Theorem 1:** The controller defined by (9) and (30), along with the estimates in (15) and (20), the update laws in (26), (47) and (48), and the observer in (42) ensure that all closed-loop signals are bounded, and the tracking error is semi-global uniformly ultimately bounded (SUUB) in the sense that  $\|\varphi\|$  uniformly converges to a ball with a constant radius, provided the control gains are selected sufficiently large based on the initial conditions of the states (see the subsequent stability analysis) and the following sufficient conditions are satisfied:

$$\alpha, \alpha_1 > \frac{1}{2}, \quad (55)$$

$$\alpha_2 > 1, \quad (56)$$

$$k_f > 4, \quad (57)$$

$$\min(\alpha_1 - \frac{1}{2}, \alpha_2 - 1, \frac{1}{8}k_f - \frac{1}{2}) > \frac{\epsilon}{2}a_5, \quad (58)$$

$$\min(\alpha - \frac{1}{2}, \frac{k}{4} - \frac{1+k_f}{2} - \frac{a_5}{2\epsilon}) > \frac{a_4^2}{k}, \quad (59)$$

$$\gamma_3(T-d) - \gamma_1 d < \ln\left(\frac{\beta_1}{\beta_2}\right), \quad (60)$$

where  $\epsilon \in \mathbb{R}$  is an arbitrary positive constant;  $a_4, a_5$  are introduced in (51);  $T, d$  are introduced in (9);  $\gamma_3 \in \mathbb{R}$  is a known, positive bounding constant;  $\gamma_1 \in \mathbb{R}$  is a constant gain that can be made arbitrarily large by selecting  $\alpha, \alpha_1, \alpha_2, k_f$ , and  $k$  in (12), (13), (30), and (43) arbitrarily large; and  $\beta_1, \beta_2 \in \mathbb{R}$  are positive constants defined as  $\beta_1 \triangleq \frac{1}{2} \min(1, \xi_0)$ ,  $\beta_2 \triangleq \frac{1}{2} \max(1, \xi_1)$ .

*Proof:* Consider the Lyapunov candidate function  $V : \mathbb{R}^7 \rightarrow \mathbb{R}$ , which is a continuously differentiable, positive definite function defined as

$$V(\varphi, t) \triangleq \frac{1}{2}e^2 + \frac{1}{2}e_1^2 + \frac{1}{2}Je_2^2 + \frac{1}{2}\tilde{x}^T \tilde{x} + \frac{1}{2}r^T r, \quad (61)$$

<sup>3</sup>For some classes of systems, the bounding function  $\rho_2$  could be selected as a constant, and a global uniformly ultimately bounded result can be obtained.

which satisfies the following inequalities

$$\beta_1 \|\varphi\|^2 \leq V \leq \beta_2 \|\varphi\|^2. \quad (62)$$

Taking the time derivative of (61), substituting the dynamics in (28) and (54), and using (35) and (38) yields

$$\begin{aligned} \dot{V}(\varphi, t) &= ee_1 - \alpha_1 e^2 + e_1 e_2 - \alpha_2 e_1^2 + e_2 f_3 + e_2 \hat{W}^T \hat{\sigma} \\ &\quad - e_2 u + r^T N_1 + r^T N_2 - kr^T r + \tilde{x}^T r - \tilde{x}^T \alpha \tilde{x}. \end{aligned}$$

The function  $V$  can be expressed in segments  $V_n(\varphi, \tau)$ , where  $V_n(\varphi, \tau) \in \mathbb{R}$  is defined as

$$V_n(\varphi, \tau) \triangleq V(\varphi(nT + \tau)), \quad (63)$$

where  $\tau \triangleq t - nT$ ,  $n \triangleq \lfloor t/T \rfloor$ . Using (29), (50), and (51) on the interval  $0 \leq \tau < d$  (i.e.,  $u = v$ ) yields

$$\begin{aligned} \dot{V}_n(\varphi, \tau) &= ee_1 - \alpha_1 e^2 + e_1 e_2 - \alpha_2 e_1^2 \\ &\quad + e_2 \rho_1 (\|z_f\|) \|z_f\| + a_2 e_2 + e_2 \hat{W}^T \hat{\sigma} \\ &\quad + r^T (\rho_2 (\|\varphi\|) \|\varphi\| + a_3) \\ &\quad - e_2 (k_f \hat{e}_2 + \hat{W}^T \hat{\sigma}) - kr^T r + \tilde{x}^T r \\ &\quad + r^T (a_4 \|z\| + a_5 \|z_f\| + a_6) - \tilde{x}^T \alpha \tilde{x}. \end{aligned}$$

Applying Young's Inequality yields

$$\begin{aligned} \dot{V}_n(\varphi, \tau) &\leq -\left(\alpha_1 - \frac{1}{2}\right) e^2 - (\alpha_2 - 1) e_1^2 \\ &\quad - \left(\frac{k_f}{8} - \frac{1}{2}\right) e_2^2 - \left(\frac{k}{4} - \frac{1+k_f}{2}\right) \|r\|^2 \\ &\quad - \left(\alpha - \frac{1}{2}\right) \|\tilde{x}\|^2 - \frac{k_f}{4} e_2^2 \\ &\quad + e_2 \rho_1 (\|z_f\|) \|z_f\| + \frac{\epsilon a_5}{2} \|z_f\|^2 \\ &\quad + \frac{a_5}{2\epsilon} \|r\|^2 - \frac{3k}{4} \|r\|^2 + r^T \rho_2 (\|\varphi\|) \|\varphi\| \\ &\quad + r^T a_4 \|z\| + r^T (a_3 + a_6) - \frac{k_f}{8} e_2^2 + a_2 e_2. \end{aligned}$$

Completing the squares and upper-bounding the result yields

$$\begin{aligned} \dot{V}_n(\varphi, \tau) &\leq -\left(\lambda_1 - \frac{\rho_1^2}{k_f}\right) \|z_f\|^2 - \lambda_2 \|z\|^2 \\ &\quad + \frac{\rho_2^2}{k} \|\varphi\|^2 + \frac{(a_3 + a_6)^2}{k} + \frac{2a_2^2}{k_f}, \end{aligned} \quad (64)$$

where  $\lambda_1, \lambda_2 \in \mathbb{R}$  are positive constants, provided the sufficient conditions in (55)–(59) are satisfied, defined as

$$\begin{aligned} \lambda_1 &\triangleq \min\left\{\alpha_1 - \frac{1}{2}, \alpha_2 - 1, \frac{k_f}{8} - \frac{1}{2}\right\} - \frac{\epsilon a_5}{2}, \\ \lambda_2 &\triangleq \min\left\{\frac{k}{4} - \frac{1+k_f}{2} - \frac{a_5}{2\epsilon}, \alpha - \frac{1}{2}\right\} - \frac{a_4^2}{k}. \end{aligned}$$

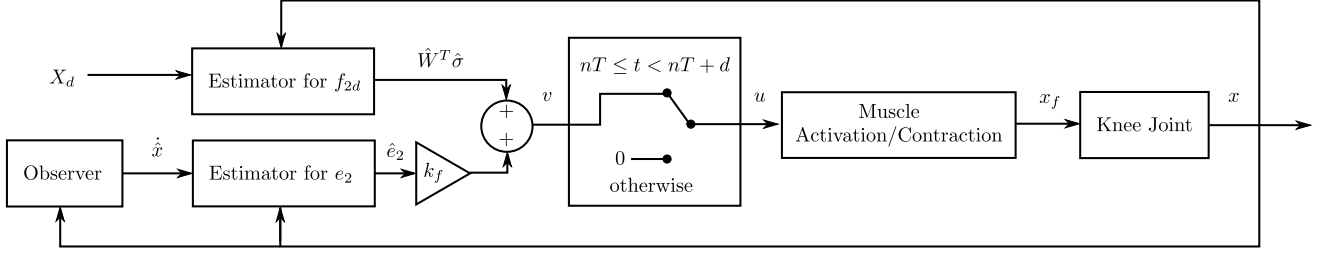


Figure 1. System block diagram.

Let two sets  $\mathcal{D}$  and  $S_{\mathcal{D}}$  be defined as

$$\mathcal{D} \triangleq \left\{ \varphi \in \mathbb{R}^7 \mid \|\varphi\| \leq \min \left( \inf \{ \rho^{-1}([\lambda_1 k k_f, \infty)) \}, \right. \right. \\ \left. \left. \inf \{ \rho_2^{-1}([\sqrt{\lambda_2 k}, \infty)) \} \right) \right\}, \quad (65)$$

$$S_{\mathcal{D}} \triangleq \left\{ \varphi \in \mathcal{D} \mid \|\varphi\| \leq \sqrt{\frac{\beta_1}{\beta_2}} \min \left( \inf \{ \rho^{-1}([\lambda_1 k k_f, \infty)) \}, \right. \right. \\ \left. \left. \inf \{ \rho_2^{-1}([\sqrt{\lambda_2 k}, \infty)) \} \right) \right\}, \quad (66)$$

where, for a set  $A \subset \mathbb{R}$ , the inverse image  $\rho^{-1}(A) \subset \mathbb{R}$  is defined as  $\rho^{-1}(A) \triangleq \{a \in \mathbb{R} \mid \rho(a) \in A\}$ , and the function  $\rho(\cdot)$  is defined as  $\rho(\cdot) \triangleq k \rho_1^2(\cdot) + k_f \rho_2^2(\cdot)$ . Using (62), (64) can be rewritten as

$$\dot{V}_n(\varphi, \tau) \leq -\gamma_1 V_n + \gamma_2, \quad \forall \varphi \in \mathcal{D}, \quad (67)$$

where  $\gamma_1, \gamma_2 \in \mathbb{R}$  are defined as

$$\gamma_1 \triangleq \frac{1}{\beta_2} \min \left\{ \lambda_1 - \frac{\rho_1^2(\|\varphi(0)\|)}{k_f} - \frac{\rho_2^2(\|\varphi(0)\|)}{k}, \right. \\ \left. \lambda_2 - \frac{\rho_2^2(\|\varphi(0)\|)}{k} \right\}, \\ \gamma_2 \triangleq \frac{(a_3 + a_6)^2}{k} + \frac{2a_2^2}{k_f}.$$

The region of attraction  $\mathcal{D}$  in (65) can be made arbitrarily large to include any initial condition by increasing the control gains  $\alpha, \alpha_1, \alpha_2, k$  and  $k_f$  (i.e., a semi-global result). Likewise, on the interval  $d \leq \tau < T$  (i.e.,  $u = 0$ ),

$$\dot{V}_n(\varphi, \tau) \leq \gamma_3 V_n(\varphi, \tau) + \gamma_4, \quad (68)$$

where  $\gamma_3, \gamma_4 \in \mathbb{R}$  are constants defined as

$$\gamma_3 \triangleq \max \{ \lambda_3, \lambda_4 \}, \quad \gamma_4 \triangleq \frac{(a_3 + a_6)^2}{k},$$

where  $\lambda_3, \lambda_4 \in \mathbb{R}$  are constants defined as

$$\lambda_3 \triangleq \max \left\{ -\left( \alpha_1 - \frac{1}{2} \right), -(\alpha_2 - 1), \left( \frac{3}{4} + a_2 + a_1 + \bar{v}_b \right) \right\} \\ + \frac{a_5^2}{k} + \frac{\rho_1^2(\|\varphi(0)\|)}{4} + \frac{\rho_2^2(\|\varphi(0)\|)}{4}, \\ \lambda_4 \triangleq \max \left\{ -\left( \alpha - \frac{1}{2} \right), -\left( \frac{k}{8} - \frac{1}{2} \right) \right\} + \frac{2a_4^2}{k} + \frac{\rho_2^2(\|\varphi(0)\|)}{4}.$$

Using (61) and (63),  $\dot{V}_n(\varphi, \tau)$  can be upper-bounded as

$$\dot{V}_n(\varphi, \tau) \leq \begin{cases} -\gamma_1 V_n(\varphi, \tau) + \gamma_2, & 0 \leq \tau < d \\ \gamma_3 V_n(\varphi, \tau) + \gamma_4, & d \leq \tau < T \end{cases},$$

which can be solved to obtain upper bounds for  $V_n(\varphi, d)$  and  $V_n(\varphi, T)$  as

$$V_n(\varphi, d) \leq \left( V_n(\varphi, 0) - \frac{\gamma_2}{\gamma_1} \right) e^{-\gamma_1 d} + \frac{\gamma_2}{\gamma_1}, \quad (69)$$

$$V_n(\varphi, T) \leq \left( V_n(\varphi, d) + \frac{\gamma_4}{\gamma_3} \right) e^{\gamma_3(T-d)} - \frac{\gamma_4}{\gamma_3}. \quad (70)$$

By using (69) and (70), and the fact that  $V_{n+1}(z, 0) = V_n(z, T)$ , the change in  $V$  across a pulse can be defined and upper-bounded as

$$\tilde{V}_n \triangleq V_{n+1}(\varphi, 0) - V_n(\varphi, 0) \\ \leq V_n(\varphi, d) e^{\gamma_3(T-d)} - V_n(\varphi, 0) \\ + \frac{\gamma_4}{\gamma_3} (e^{\gamma_3(T-d)} - 1), \\ \leq V_n(\varphi, 0) (e^{-\gamma_1 d} e^{\gamma_3(T-d)} - 1) \\ + \frac{\gamma_2}{\gamma_1} (1 - e^{-\gamma_1 d}) e^{\gamma_3(T-d)} \\ + \frac{\gamma_4}{\gamma_3} (e^{\gamma_3(T-d)} - 1). \quad (71)$$

To ensure that  $\|\varphi(nT)\| > \|\varphi((n+1)T)\|$ ,  $\tilde{V}_n$  must satisfy the following condition:

$$\tilde{V}_n < V_n(\varphi, 0) \frac{\beta_1 - \beta_2}{\beta_2}. \quad (72)$$

To satisfy (72), it is sufficient to demonstrate that (71) satisfies

$$\tilde{V}_n \leq V_n(\varphi, 0) (e^{-\gamma_1 d} e^{\gamma_3(T-d)} - 1) \\ + \frac{\gamma_2}{\gamma_1} (1 - e^{-\gamma_1 d}) e^{\gamma_3(T-d)} \\ + \frac{\gamma_4}{\gamma_3} (e^{\gamma_3(T-d)} - 1) \\ < V_n(\varphi, 0) \frac{\beta_1 - \beta_2}{\beta_2}. \quad (73)$$

If the condition in (60) is satisfied and  $V(\varphi(nT)) > \beta_1 \bar{d}^2$ , where  $\bar{d} \in \mathbb{R}$  is defined as

$$\bar{d} \triangleq \sqrt{\frac{\frac{\gamma_4}{\gamma_3} (1 - e^{-\gamma_3(T-d)}) + \frac{\gamma_2}{\gamma_1} (1 - e^{-\gamma_1 d})}{\beta_1 \left( \frac{\beta_1}{\beta_2} e^{-\gamma_3(T-d)} - e^{-\gamma_1 d} \right)}}, \quad (74)$$

then  $V(\varphi(nT)) < V(\varphi((n+1)T))$ , i.e.,

$$V(\varphi(0)) > V(\varphi(T)) > V(\varphi(2T)) > \dots \quad (75)$$

The size of  $\bar{d}$  is based on the period, pulse width, and control gains.

Given (61), (62), (65), and (75),  $e$  is SUUB [40, Theorem 4.18] in the sense that

$$|e| \leq \|\varphi\| < \bar{d}, \forall t \geq \bar{T}(\bar{d}, \|\varphi(0)\|), \forall \|\varphi(0)\| \in S_{\mathcal{D}},$$

where  $\bar{T}(\bar{d}, \|\varphi(0)\|) \in \mathbb{R}$  is a positive constant that denotes the ultimate time to reach the ball. ■

*Remark 1.* Based on (60) and (74), the interplay between the modulation strategy and the controller can be determined. To minimize muscle fatigue, one is motivated to decrease the stimulation frequency (i.e., increase  $T$ ; see [41]–[43]). From (60) and (74), decreasing the stimulation frequency indicates that the control gains should be selected larger (making  $\gamma_1$  larger) to maintain a similar level of steady state tracking performance. If the frequency is increased (leading to accelerated muscle fatigue), then the control gains may be selected lower to maintain a similar level of tracking performance.

## VI. EXPERIMENTS

The controller defined by (9) and (30), along with the estimates in (15) and (20), the update laws in (26), (47) and (48), and the observer in (42) was implemented on five able-bodied volunteers with written informed consent approved by the University of Florida Institutional Review Board. The purpose of the experiments was to evaluate the control performance and to investigate the interplay between stimulation frequency and control gains described in Remark 1. In the experiments, each subject was instructed to sit on a customized leg extension machine, described in [21], with an additional free swinging rigid arm which was attached to the subject’s shank. The arm’s center of rotation was aligned with the subject’s lateral femoral condyle for each trial, allowing the angular position of the arm to coincide with the knee angle. An optical encoder was used to measure the angular position  $q$  of the rigid arm at a sampling rate of 1 kHz. The angular velocity  $\dot{q}$  was obtained using backward differencing methods without filtering. Bipolar, self-adhesive 3” × 5” PALS<sup>®</sup> oval electrodes<sup>4</sup> were used to deliver the electrical stimulus. One electrode was placed over the distal-medial portion of the quadriceps femoris muscle group and the other was placed over the proximal-lateral portion. The electrical stimulation was delivered through a custom built stimulator as **monophasic, rectangular pulses** with a constant pulse width of  $d = 400\mu\text{s}$  and pulse frequency ( $f = \frac{1}{T}$ ) of 25Hz and 60Hz. **The controller was implemented with a neural network (i.e., five sigmoid neurons) along with two sets of parameters: low frequency with high gains (LFHG) and high frequency with low gains (HFLG).** First, the control

gains were tuned for each subject at a frequency of 60 Hz (high frequency) until a set of gains were found that yielded satisfactory performance (high gains). The gain tuning adopted was based on a trial-and-error approach, where  $\gamma_1$  was increased by simultaneously increasing  $k$ ,  $k_f$ ,  $\alpha_1$ , and  $\alpha_2$ . Then, LFHG was defined as using the controller with the high gains implemented at a frequency of 25 Hz (low frequency). Finally, HFLG was defined as using the controller with low gains, defined as 20% less than the high gains, implemented at high frequency (60 Hz). The amplitude of the electrical pulses was modulated by the output of the controller.

For each trial, the subjects were instructed to relax as much as possible to reduce voluntary participation in the tracking task, and they were given no indication of their tracking performance during the experiment. Each session was 20 seconds long and between sessions the subjects were given at least five minutes of rest to minimize the effect of muscle fatigue on the results.

*Remark 2.* Able-bodied subjects and subjects with upper motor neuron lesions can both fit the developed model. However, specific disease or injury conditions can lead to differences in performance (e.g., rapid fatigue, spasticity, etc.). The developed controller is analyzed in the presence of general disturbance terms that can be used to model such effects. While the experiments only demonstrate the controller’s performance in able-bodied individuals, and hence demonstrate efficacy of the controller and relationships between the controller and modulation parameters, results will potentially vary when the controller is applied to specific disease or injury populations.

Without loss of generality, the desired trajectory was designed to be sinusoidal<sup>5</sup> with a period of 2.5 seconds, ranging from 5° to 60° from the subject’s rest position, **where the angle between the shank and the vertical line is 0°**. Each subject performed eight repetitions over the course of the 20 second trial. To validate the interplay between control gains and stimulation frequencies stated in Remark 1, two different control strategies were employed: low frequency with high gains (LFHG) and high frequency with low gains (HFLG). **The neural network used is constructed based on five sigmoid neurons (i.e.,  $n_0 = 5$ ) with one hidden layer**, and the control gain tuning adopted is based on a trial-and-error approach. A pulse frequency of 25 Hz was used for LFHG, and 60 Hz was used for HFLG. For LFHG,  $\gamma_1$  was increased by simultaneously increasing  $k$ ,  $k_f$ ,  $\alpha_1$ , and  $\alpha_2$  until satisfactory performance was achieved **(i.e., until the steady-state tracking error response was approximately five degrees RMS or less, similar to the results such as [44], [45])**. For HFLG, low gains were defined as 15-20% less than the gains used for LFHG.

Representative results for one individual are presented in

<sup>4</sup>Surface electrodes for the study were provided compliments of Axelgaard Manufacturing Co., Ltd.

<sup>5</sup>The tracking performance of the closed-loop system with different desired trajectories, **including multiple frequencies**, remains the same provided that Assumption 1 is satisfied.

Figures 2, which illustrates the tracking errors, desired and measured angles from the representative subject's trial using HFLG and LFHG approaches, and the control inputs. The RMS and normalized root mean square (NRMS) tracking errors of all five subjects are summarized in Table I-III. The range of voltages applied to all five subjects is 15-34 Volts. (b)-(c) of Figure 2 depict the tracking errors and desired versus measured angles from a representative subject's trial. During the transient period (i.e., 0-10 seconds), the tracking errors are bounded, oscillating trajectories, implying that the system is stable. However, the oscillations make comparison of HFLG and LFHG approaches difficult so that the RMS tracking errors were calculated over each 2.5 seconds period of the desired trajectory. For all subjects, the HFLG strategy consistently resulted in higher transient error when compared to LFHG strategy, but the steady state RMS tracking errors of both strategies behaved similarly, reflecting the predicted interplay between the stimulation frequencies and control gains derived in (74). Control inputs from the two approaches for the representative subject is given in (d). For all subjects, the LFHG approach yielded a higher control input voltage, but the tracking errors of the two approaches were similar. One interpretation of the results is that the high frequency input generates more muscle force output than the lower frequency, thereby requiring less control input voltage to achieve similar tracking performance.

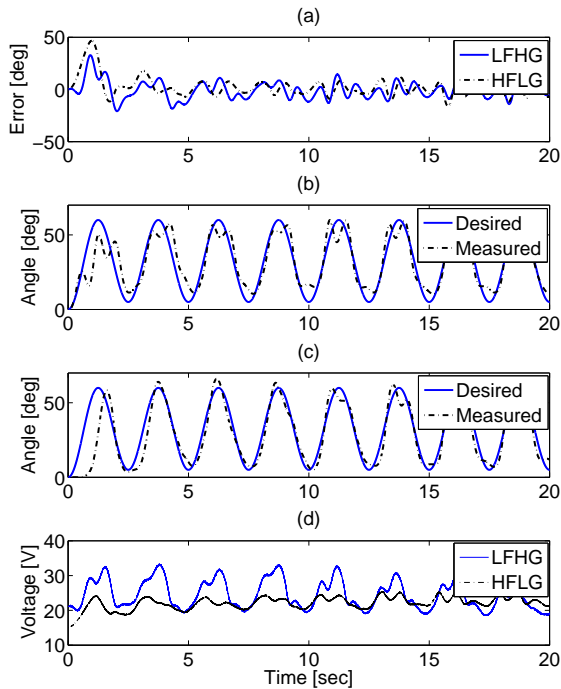


Figure 2. (a) Tracking errors errors from the two protocols with the representative subject. (b) Desired vs. measured joint angles with the representative subject using LFHG strategy. (c) Desired vs. measured joint angles with the representative subject using HFLG strategy. (d) Comparison of control inputs for the two protocols with the representative subject.

Table I  
COMPARISON OF AVERAGE RMS TRACKING ERRORS FOR ALL FIVE SUBJECTS WITH MEAN VALUES, MEDIAN VALUES, AND STANDARD DEVIATIONS, AND NRMS TRACKING ERRORS.

Subject	0-20 seconds			
	RMS (deg.)		NRMS (%)	
	LFHG	HFLG	LFHG	HFLG
1	6.3	6.7	19	17
2	9.5	12.7	15	15
3	7.3	8.3	13	12
4	6.9	7.6	16	11
5	6.1	5.7	16	17
Mean	7.22	8.2	N/A	N/A
Median	6.9	7.6	N/A	N/A
SD	1.36	2.70	N/A	N/A

Table II  
COMPARISON OF TRANSIENT RMS TRACKING ERRORS FOR ALL FIVE SUBJECTS WITH MEAN VALUES, MEDIAN VALUES, AND STANDARD DEVIATIONS, AND TRANSIENT NRMS TRACKING ERRORS.

Subject	0-10 seconds			
	RMS (deg.)		NRMS (%)	
	LFHG	HFLG	LFHG	HFLG
1	7.1	8.7	22	23
2	15.5	21.3	25	25
3	10	12.4	19	21
4	9.4	14.3	23	22
5	7.2	7.2	20	20
Mean	9.84	12.78	N/A	N/A
Median	9.4	12.4	N/A	N/A
SD	3.41	5.54	N/A	N/A

Table III  
COMPARISON OF STEADY STATE RMS TRACKING ERRORS FOR ALL FIVE SUBJECTS WITH MEAN VALUES, MEDIAN VALUES, AND STANDARD DEVIATIONS, AND STEADY STATE NRMS TRACKING ERRORS.

Subject	10-20 seconds			
	RMS (deg.)		NRMS (%)	
	LFHG	HFLG	LFHG	HFLG
1	5.4	3.7	23	20
2	8.7	12.1	24	25
3	6.0	6.1	21	22
4	4.8	4.9	24	24
5	4.8	3.7	20	22
Mean	5.94	6.1	N/A	N/A
Median	5.4	4.9	N/A	N/A
SD	1.62	3.5	N/A	N/A

Tables I-III summarize the experimental results for the LFHG and HFLG protocols by the RMS and NRMS tracking errors calculated over the entire trials (0-20 seconds), transient period (0-10 seconds), and during steady state (10-20 seconds), respectively. While HFLG appears to have a greater RMS error over the entire trial (see Tables I-III), a Wilcoxon Signed-Rank test on the paired data resulted in a  $P$ -value of 0.138. Thus, one cannot conclude at a

significance level of 0.05 that there is a significant difference between the the HFLG and LFGH protocols in terms of the median RMS tracking errors over the entire duration of the trials (see Table I). In Table II, the transient performances of both protocols are compared with a Wilcoxon Signed-Rank test on the paired data resulted in a  $P$ -value of 0.10, which one cannot conclude at a significance level of 0.05 that there is a significant difference between the the HFLG and LFGH protocols. Similarly, both protocols resulted in similar steady state RMS tracking errors (see Table III). A Wilcoxon Signed-Rank test on the paired data during steady state resulted in a  $P$ -value of 1.0, further indicating that the LFGH and HFLG protocols result in statistically similar steady state performance, as concluded in Remark 1. The control gains implemented in the experiments are listed in Table IV, and the peak, mean, and median values of the control efforts are summarized in Table V.

Table IV  
CONTROL GAINS USED FOR THE TWO STRATEGIES WITH THE FIVE SUBJECTS.

Subject	Strategy	$\alpha$	$\alpha_1$	$\alpha_2$	$k_f$	$k$
1	LFGH	10	20	20	0.026	50
	HFLG	8	16	16	0.021	40
2	LFGH	10	9	9	0.013	25
	HFLG	8	7.2	7.2	0.01	20
3	LFGH	10	22	22	0.019	40
	HFLG	8	18	18	0.015	35
4	LFGH	10	22	22	0.019	40
	HFLG	8	15	15	0.015	30
5	LFGH	10	27	27	0.021	30
	HFLG	8	22	22	0.019	40

Table V  
PEAK, MEAN, AND MEDIAN VALUE OF THE CONTROL INPUTS OF THE TWO STRATEGIES WITH THE FIVE SUBJECTS.

Subject	Strategy	Peak (Volts)	Mean (Volts)	Median (Volts)
1	LFGH	30	24.6	24
	HFLG	26.7	23.2	22.9
2	LFGH	22.8	20.7	20.6
	HFLG	21.4	19.9	18.9
3	LFGH	33.3	24	23.5
	HFLG	27.3	23	23
4	LFGH	30	26	27.5
	HFLG	26.2	22.6	22.6
5	LFGH	34	26.5	26.1
	HFLG	29.4	24.6	24.6

## VII. CONCLUSION

An identification-based closed-loop NMES controller was designed based on an uncertain muscle activation model with a amplitude-modulated control input. Based on Lyapunov stability analysis methods for switched systems, the controller is proven to ensure SUUB tracking, provided sufficient conditions on the control gains and stimulation modulation parameters are satisfied. To support the main result of

this paper, experiments on five able-bodied volunteers are implemented. The theoretical link between frequency and the control gains was demonstrated in the sense that, as discussed in Remark 1, higher control gains paired with a low frequency modulation strategy yielded similar tracking performance to a high frequency modulation scheme with lower control gains. Future work will seek to extend these results to functional activities involving multiple muscle groups and several degrees of freedom (e.g., cycling, walking).

## REFERENCES

- [1] G. M. Lyons, T. Sinkjaer, J. H. Burridge, and D. J. Wilcox, "A review of portable fes-based neural orthoses for the correction of drop foot," *IEEE Trans. Neur. Sys. and Rehab. Eng.*, vol. 10, no. 4, pp. 260–279, Dec. 2002.
- [2] J. J. Abbas and H. J. Chizeck, "Feedback control of coronal plane hip angle in paraplegic subjects using functional neuromuscular stimulation," *IEEE Trans. Biomed. Eng.*, vol. 38, no. 7, pp. 687–698, July 1991.
- [3] N. Lan, P. E. Crago, and H. J. Chizeck, "Control of end-point forces of a multijoint limb by functional neuromuscular stimulation," *IEEE Trans. Biomed. Eng.*, vol. 38, no. 10, pp. 953–965, October 1991.
- [4] N. Lan, P. E. Crago, and H. J. Chizeck, "Feedback control methods for task regulation by electrical stimulation of muscles," *IEEE Trans. Biomed. Eng.*, vol. 38, no. 12, pp. 1213–1223, December 1991.
- [5] T. Schauer, N. O. Negård, F. Previdi, K. J. Hunt, M. H. Fraser, E. Ferchland, and J. Raisch, "Online identification and nonlinear control of the electrically stimulated quadriceps muscle," *Control Eng. Pract.*, vol. 13, no. 9, pp. 1207–1219, September 2005.
- [6] N. Lan, H.-Q. Feng, and P. E. Crago, "Neural network generation of muscle stimulation patterns for control of arm movements," *IEEE Trans. Rehabil. Eng.*, vol. 2, no. 4, pp. 213–224, December 1994.
- [7] J. J. Abbas and H. J. Chizeck, "Neural network control of functional neuromuscular stimulation systems: computer simulation studies," *IEEE Trans. Biomed. Eng.*, vol. 42, no. 11, pp. 1117–1127, Nov. 1995.
- [8] D. Graupe and H. Kordylewski, "Artificial neural network control of FES in paraplegics for patient responsive ambulation," *IEEE Trans. Biomed. Eng.*, vol. 42, no. 7, pp. 699–707, July 1995.
- [9] G.-C. Chang, J.-J. Lub, G.-D. Liao, J.-S. Lai, C.-K. Cheng, B.-L. Kuo, and T.-S. Kuo, "A neuro-control system for the knee joint position control with quadriceps stimulation," *IEEE Trans. Rehabil. Eng.*, vol. 5, no. 1, pp. 2–11, Mar. 1997.
- [10] J. Riess and J. J. Abbas, "Adaptive neural network control of cyclic movements using functional neuromuscular stimulation," *IEEE Trans. Neural Syst. Rehabil. Eng.*, vol. 8, no. 1, pp. 42–52, March 2000.
- [11] H. Kordylewski and D. Graupe, "Control of neuromuscular stimulation for ambulation by complete paraplegics via artificial neural networks," *Neural Res.*, vol. 23, no. 5, pp. 472–481, July 2001.
- [12] D. G. Zhang and K. Y. Zhu, "Simulation study of FES-assisted standing up with neural network control," in *Proc. Annu. Int. Conf. IEEE Eng. Med. Biol. Soc.*, vol. 2, San Francisco, California, September 2004, pp. 4877–4880.
- [13] J. P. Giuffrida and P. E. Crago, "Functional restoration of elbow extension after spinal-cord injury using a neural network-based synergistic FES controller," *IEEE Trans. Neural Syst. Rehabil. Eng.*, vol. 13, no. 2, pp. 147–152, June 2005.
- [14] K. Kurosawa, R. Futami, T. Watanabe, and N. Hoshimiya, "Joint angle control by FES using a feedback error learning controller," *IEEE Trans. Neural Syst. Rehabil. Eng.*, vol. 13, no. 3, pp. 359–371, September 2005.
- [15] A. Pedrocchi, S. Ferrante, E. De Momi, and G. Ferrigno, "Error mapping controller: a closed loop neuroprosthesis controlled by artificial neural networks," *J. Neuroeng. Rehabil.*, vol. 3, no. 1, p. 25, October 2006.
- [16] D. Kim, W. Mackunis, N. Fitz-Coy, and W. E. Dixo, "Precision ipacs in the presence of dynamic uncertainty," in *Proc. IEEE Conf. Decis. Control*, Shanghai, China, January 2009, pp. 5959–5964.
- [17] A. Ajoudani and A. Erfanian, "A neuro-sliding-mode control with adaptive modeling of uncertainty for control of movement in paralyzed limbs using functional electrical stimulation," *IEEE Trans. Biomed. Eng.*, vol. 56, no. 7, pp. 1771–1780, Jul. 2009.

- [18] J. L. Lujan and P. E. Crago, "Automated optimal coordination of multiple-DOF neuromuscular actions in feedforward neuroprostheses," *IEEE Trans. Biomed. Eng.*, vol. 56, no. 1, pp. 179–187, January 2009.
- [19] Y.-L. Chen, W.-L. Chen, C.-C. Hsiao, T.-S. Kuo, and J.-S. Lai, "Development of the FES system with neural network + PID controller for the stroke," in *Proc. IEEE Int. Symp. Circuits Syst.*, May 23–26, 2005, pp. 5119–5121.
- [20] N. Sharma, C. M. Gregory, M. Johnson, and W. E. Dixon, "Modified neural network-based electrical stimulation for human limb tracking," in *Proc. IEEE Int. Symp. Intell. Control*, San Antonio, Texas, September 2008, pp. 1320–1325.
- [21] N. Sharma, K. Stegath, C. M. Gregory, and W. E. Dixon, "Nonlinear neuromuscular electrical stimulation tracking control of a human limb," *IEEE Trans. Neural Syst. Rehabil. Eng.*, vol. 17, no. 6, pp. 576–584, June 2009.
- [22] Q. Wang, N. Sharma, M. Johnson, and W. E. Dixon, "Asymptotic optimal control of neuromuscular electrical stimulation," *IEEE Trans. Cybern.*, vol. 43, no. 6, pp. 1710–1718, 2013.
- [23] Q. Wang, N. Sharma, M. Johnson, and W. E. Dixon, "Adaptive inverse optimal neuromuscular electrical stimulation," in *Proc. IEEE Int. Symp. Intell. Control*, Yokohama, Japan, September 2010, pp. 1287–1292.
- [24] N. Sharma, P. Patre, C. Gregory, and W. E. Dixon, "Nonlinear control of NMES: Incorporating fatigue and calcium dynamics," in *Proc. ASME Dyn. Syst. Control Conf.*, Hollywood, CA, October 2009, pp. 705–712.
- [25] S.-J. Kim, M. D. Fairchild, A. Iarkov, J. J. Abbas, and R. Jung, "Adaptive control of movement for neuromuscular stimulation-assisted therapy in a rodent model," *IEEE Trans Biomed Eng*, vol. 56, no. 2, pp. 452–461, February 2009.
- [26] H.-R. Kobravi and A. Erfanian, "Decentralized adaptive robust control based on sliding mode and nonlinear compensator for the control of ankle movement using functional electrical stimulation of agonist-antagonist muscles," *J. Neural Eng.*, vol. 6, no. 4, pp. 1–10, July 2009.
- [27] V. Nekoukar and A. Erfanian, "A decentralized modular control framework for robust control of fes-activated walker-assisted paraplegic walking using terminal sliding mode and fuzzy logic control," *IEEE Trans. Biomed. Eng.*, vol. 59, no. 10, pp. 2818–2827, October 2012.
- [28] P. H. Peckham and J. S. Knutson, "Functional electrical stimulation for neuromuscular applications," *Annu. Rev. Biomed. Eng.*, vol. 7, pp. 327–360, March 2005.
- [29] T. Kesar, L.-W. Chou, and S. A. Binder-Macleod, "Effects of stimulation frequency versus pulse duration modulation on muscle fatigue," *J. Electromyogr. Kinesiol.*, vol. 18, no. 4, pp. 662–671, Aug 2008.
- [30] Q. Wang, H. Dinh, M. Bellman, and W. E. Dixon, "Neuromuscular electrical stimulation with an uncertain muscle contraction model," in *Proc. Dyn. Sys. Contr. Conf.*, Ft. Lauderdale, Florida, October 2012, pp. 519–528.
- [31] M. Ferrarin and A. Pedotti, "The relationship between electrical stimulus and joint torque: A dynamic model," *IEEE Trans. Rehabil. Eng.*, vol. 8, no. 3, pp. 342–352, September 2000.
- [32] W. L. Buford, J. F. M. Ivey, J. D. Malone, R. M. Patterson, G. L. Peare, D. K. Nguyen, and A. A. Stewart, "Muscle balance at the knee - moment arms for the normal knee and the ACL - minus knee," *IEEE Trans. Rehabil. Eng.*, vol. 5, no. 4, pp. 367–379, December 1997.
- [33] T. S. Buchanan, D. G. Lloyd, K. Manal, and T. F. Besier, "Neuromusculoskeletal modeling: Estimation of muscle forces and joint moments and movements from measurements of neural command," *J. Appl. Biomech*, vol. 20, no. 4, pp. 367–395, 2004.
- [34] Y. Giat, J. Mizrahi, and M. Levy, "A musculotendon model of the fatigue profiles of paralyzed quadriceps muscle under FES," *IEEE Trans. Biomed. Eng.*, vol. 40, no. 7, pp. 664–674, July 1993.
- [35] R. Nathan and M. Tavi, "The influence of stimulation pulse frequency on the generation of joint moments in the upper limb," *IEEE Trans. Biomed. Eng.*, vol. 37, no. 3, pp. 317–322, March 1990.
- [36] T. Watanabe, R. Futami, N. Hoshimiya, and Y. Handa, "An approach to a muscle model with a stimulus frequency-force relationship for FES applications," *IEEE Trans. Rehabil. Eng.*, vol. 7, no. 1, pp. 12–18, March 1999.
- [37] G. Cybenko, "Approximation by superpositions of a sigmoidal function," *Math. Control Signals Syst.*, vol. 2, no. 4, pp. 303–314, December 1989.
- [38] F. L. Lewis, R. Selmic, and J. Campos, *Neuro-Fuzzy Control of Industrial Systems with Actuator Nonlinearities*. Philadelphia, PA, USA: Society for Industrial and Applied Mathematics, 2002.
- [39] W. E. Dixon, A. Behal, D. M. Dawson, and S. Nagarkatti, *Nonlinear Control of Engineering Systems: A Lyapunov-Based Approach*. Birkhauser: Boston, 2003.
- [40] H. K. Khalil, *Nonlinear Systems*, 3rd ed. Upper Saddle River, NJ, USA: Prentice Hall, 2002.
- [41] S. A. Binder-Macleod, E. E. Halden, and K. A. Jungles, "Effects of stimulation intensity on the physiological responses of human motor units," *Med. Sci. Sports. Exerc.*, vol. 27, no. 4, pp. 556–565, Apr 1995.
- [42] D. A. Jones, B. Bigland-Ritchie, and R. H. T. Edwards, "Excitation frequency and muscle fatigue: Mechanical responses during voluntary and stimulated contractions," *Exp. Neurol.*, vol. 64, no. 2, pp. 401–413, May 1979.
- [43] C. M. Gregory, W. E. Dixon, and C. S. Bickel, "Impact of varying pulse frequency and duration on muscle torque production and fatigue," *Muscle Nerve*, vol. 35, no. 4, pp. 504–509, April 2007.
- [44] N. Sharma, C. Gregory, and W. E. Dixon, "Predictor-based compensation for electromechanical delay during neuromuscular electrical stimulation," *IEEE Trans. Neural Syst. Rehabil. Eng.*, vol. 19, no. 6, pp. 601–611, 2011.
- [45] N. Sharma, C. M. Gregory, M. Johnson, and W. E. Dixon, "Closed-loop neural network-based nmes control for human limb tracking," *IEEE Trans. Control Syst. Tech.*, vol. 20, no. 3, pp. 712–725, 2012.